Optimal Mission Profile for Low-Boom Supersonic Aircraft

Wu Li*, Karl Geiselhart†, and Christopher Eggert†
NASA Langley Research Center, Hampton, Virginia 23681, USA

I. Introduction

THE ban on overland supersonic flights is a key barrier to the development of commercial supersonic aircraft. To help lift this ban, NASA has been developing low-boom technologies that will enable a commercially successful supersonic transport to fly overland with a quiet sonic thump on the ground, instead of a loud sonic boom. The X-59, NASA's quiet supersonic experimental aircraft [1,2], has been designed using low-boom shaping technologies based on computational fluid dynamics (CFD) to demonstrate a sonic thump of about 75 perceived levels in decibels (PLdB) [3] on the ground.

Although low-boom shaping technologies have reasonably matured, a simultaneous achievement of design goals for aerodynamic efficiency and low-boom shaping of the outer mold line (OML) of a commercial supersonic transport is still extremely challenging. The recent work [4,5] using a multiobjective multidisciplinary optimization (MDO) method called the block coordinate optimization (BCO) method demonstrated success on that front in the conceptual design phase. The low-boom constraint (see Eq. (4) in Ref. [4]) enforced by BCO uses the NASA N+3 low-boom goal [6] conceptually at the start of overland cruise (SOC). It is quantified by a close match between the reversed equivalent area ($A_{e,r}$) [7] of the supersonic aircraft and an $A_{e,r}$ target with an undertrack sonic boom ground noise level below 70. The specified mission performance goals maintained by BCO include a low-boom overland mission for airport pairs over the continental US and an unrestricted overwater mission for transatlantic commercial flights. The BCO method dissects a tightly coupled MDO problem for achieving both the low-boom and mission performance goals into several weakly coupled and solvable optimization subproblems. These optimization subproblems are solved successively and repeatedly to find a supersonic transport that satisfies both the low-boom constraint and the specified mission performance requirements, even when an aeropropulsive CFD simulation is required for sonic boom analysis [5].

Achieving a low-boom ground noise level goal in the undertrack direction at SOC is only the first step in the development of a low-boom supersonic transport. In reality, a low-boom supersonic transport must achieve a low-boom ground noise level goal in all azimuthal directions for the entire mission trajectory. A detailed study of low-boom characteristics of a supersonic aircraft in all azimuthal directions for the entire mission trajectory was performed for JAXA's conceptual low-boom supersonic transport [8]. A sensitivity analysis shows that the range and maximum sonic boom ground noise level depend on the mission trajectory (see Figs. 16 and 17 in Ref. [8]).

This paper uses a simple method to determine an optimal mission profile for low-boom cruise of any low-boom aircraft, which will be called the low-boom mission profile (see Sec. II). The low-boom mission profile uses a fixed angle of attack (AoA), when possible, for the cruise segment to simultaneously increase the cruise range and reduce sonic boom ground noise levels of a low-boom aircraft. The fixed AoA is determined by the cruise condition for the low-boom shaping of the aircraft. Only once the aircraft reaches its cruise ceiling is the AoA reduced to account for decreasing cruise weight since changes in AoA might have a detrimental effect on the designed low-boom characteristics. Our main contribution is to numerically verify that the nondimensional overpressure (dp/p) in the undertrack direction at three body lengths (3BL) below a supersonic aircraft is approximately invariant with altitude when the aircraft OML, cruise Mach, and AoA are fixed. This verification has been done using both inviscid and viscous CFD solvers. This property of dp/p enables the verification of optimality of the fixed AoA trajectory for maintaining the low-boom characteristics of a supersonic aircraft for the entire cruise segment, even though the aircraft OML shape is only designed to be low boom at SOC. A new analysis method is proposed for the assessment of low-boom characteristics of a low-boom concept at the end of cruise (see Sec. III). This analysis method shows that a low-boom concept designed only for low boom at SOC could potentially retain the designed low-boom characteristics at the end of cruise when the low-boom mission profile is used.

II. Optimality of Fixed AoA Trajectory for Low-Boom Supersonic Aircraft

An aircraft concept with an overland cruise Mach of 1.7 and 46 passengers (PAX) (see Fig. 1) is selected for demonstration of the optimality of the fixed AoA trajectory for low-boom supersonic aircraft. This Mach 1.7 46-PAX

* Senior Research Engineer, Aeronautics Systems Analysis Branch
† Aerospace Engineer, Aeronautics Systems Analysis Branch

concept is derived from a low-boom concept with 40 passengers, referred to as the Mach 1.7 40-PAX concept [5], which was designed to approximately match an $A_{e,r}$ target of 69.9 PLdB in the undertrack direction at SOC [4]. The Mach 1.7 46-PAX concept has the same OML as the Mach 1.7 40-PAX concept. The low-boom cruise altitude and maximum takeoff gross weight of the Mach 1.7 46-PAX concept are derived iteratively to ensure that (i) its AoA at SOC is 2.3 deg (which is the AoA for the Mach 1.7 40-PAX concept at SOC) and (ii) its undertrack $A_{e,r}$ matches an $A_{e,r}$ target with an undertrack sonic boom ground noise level below 70 PLdB at SOC (see the PLdB value of the target signature in Fig. 2).

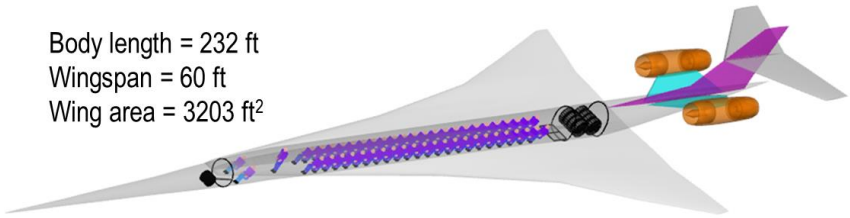

Fig. 1 Mach 1.7 46-PAX low-boom concept.

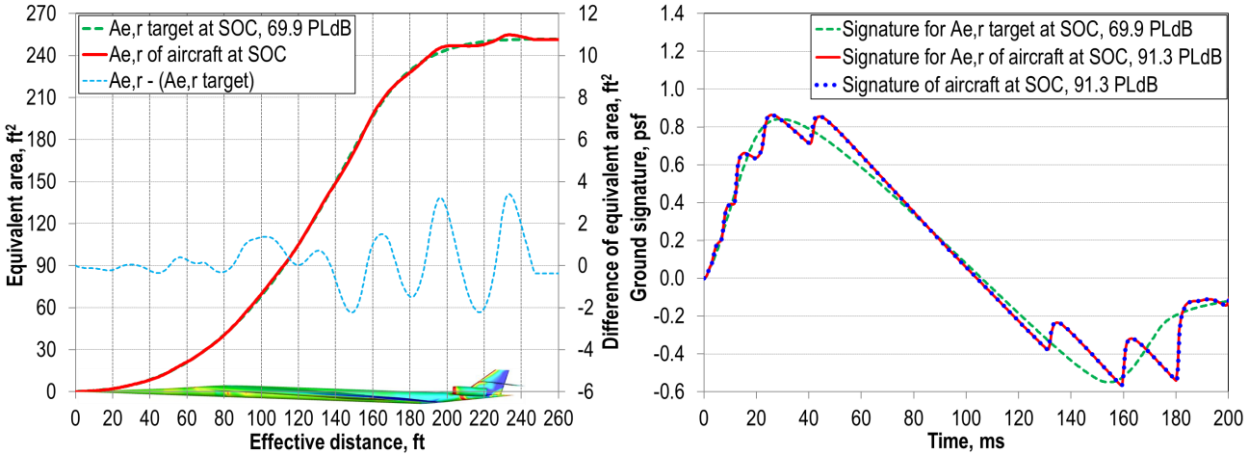

Fig. 2 Equivalent areas and undertrack ground signatures of the Mach 1.7 46-PAX concept and its target.

The weight and mission performance data are calculated using the Flight Optimization System (FLOPS) [9]. The Euler solver Cart3D [10] is the primary CFD tool for calculation of *dp/p* in this paper. See Ref. [4] for details on how FLOPS and Cart3D are used to generate the analysis results, as well as details on the sonic boom analysis methods to compute the ground signatures of the aircraft and the $A_{e,r}$ target.

For any inviscid CFD solver and fixed OML with flow-through nacelles, an aircraft's undertrack *dp/p* at 3BL below the aircraft is approximately invariant with respect to altitude change (see Fig. 3a) as long as the AoA [or lift coefficient (C_L)] and cruise Mach number are fixed. So, if the undertrack $A_{e,r}$ of a supersonic aircraft is an acceptable inverse design of a certain $A_{e,r}$ target with a ground noise level of 69.9 PLdB at its SOC, then this aircraft will have approximately the same undertrack $A_{e,r}$ at higher altitudes, provided that it is flown at the same AoA. Moreover, the same target $A_{e,r}$ distribution at a higher cruise altitude will produce a ground noise level that is lower than the original 69.9 PLdB. For example, the Mach 1.7 46-PAX concept with an AoA of 2.3 deg is an acceptable inverse design for the $A_{e,r}$ target in Fig. 2 at its SOC altitude of 51,740 ft. The same aircraft, when flown at its cruise ceiling of 60,000 ft but maintaining an AoA of 2.3 deg, produces a lower target value of undertrack sonic boom ground noise level of 67.4 PLdB (see Fig. 3b).

Because the analysis results in Fig. 3a are generated using the Euler solver Cart3D, a Reynolds-averaged Navier-Stokes CFD solver FUN3D [11] is also used to verify the approximate invariance of *dp/p* with respect to altitude change. For the Mach 1.7 46-PAX concept at AoA = 2.3 deg, a full-span cylindrical core grid of tetrahedra near the aircraft is generated using HeldenMesh [12] and a prismatic collar grid [13] is generated for computing *dp/p* at 3BL below the aircraft. The core and collar grids are combined into the grid that is used for CFD analysis in FUN3D. It has 44.7M nodes and 183.8M elements. The *dp/p* values are extracted at 1144 points along a line located 3BL directly beneath the aircraft. The FUN3D solutions use the Spalart–Allmaras turbulence model [14], Roe's flux scheme [15], and the van Leer limiter [16]. The FUN3D grid on the symmetry plane and the computed *dp/p* distributions are plotted

in Fig. 4. The FUN3D *dp/p* distributions are also approximately identical for different altitudes (see Fig. 4b), with the corresponding Reynolds numbers from 1.25M to 3.26M. This confirms that *dp/p* at 3BL below the aircraft is approximately invariant with respect to altitude change.

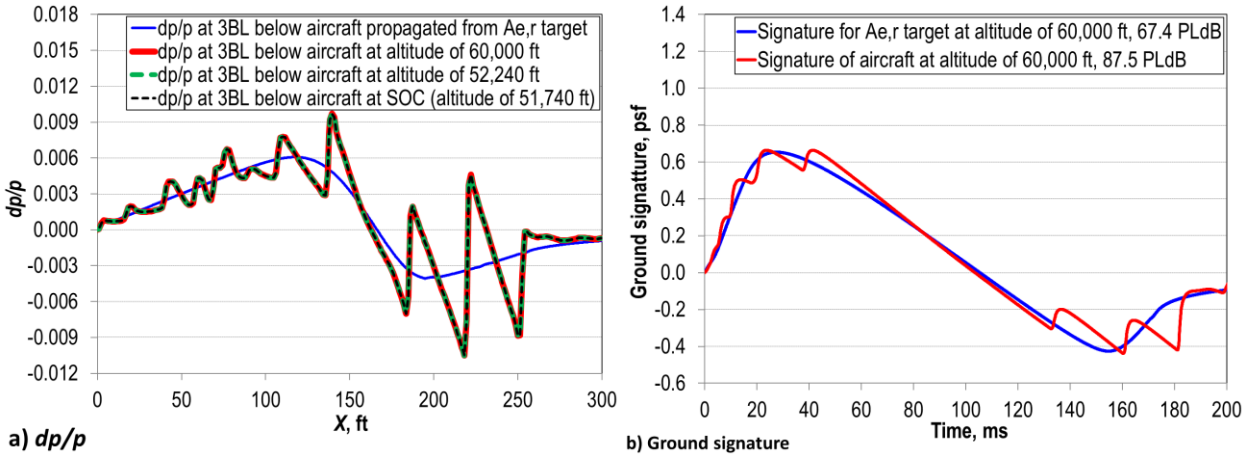

Fig. 3 Euler *dp/p* for various altitudes and undertrack signatures at cruise ceiling when AoA = 2.3 deg.

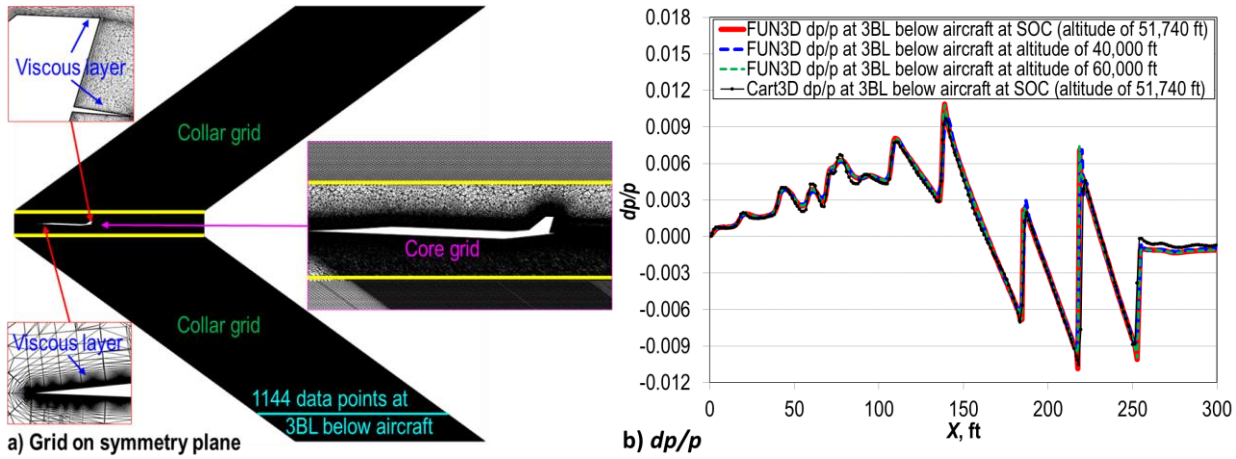

Fig. 4 FUN3D grid on symmetry plane *y* = 0 and *dp/p* for various altitudes when AoA = 2.3 deg.

Figure 4b indicates that the viscosity has marginal effects on the off-body *dp/p* calculation if the aircraft OML, cruise Mach, and AoA are fixed in the CFD analysis. The noticeable differences in *dp/p* (see Fig. 4b) are perhaps mainly due to the different grid resolutions between the inviscid and viscous grids. The Cartesian grid for the Cart3D *dp/p* in Fig. 3a is generated using the method in Ref. [17]. It is a half-span grid on $y \geq 0$, with about 35M cells and 388 data points to define *dp/p* at 3BL below the aircraft at AoA = 2.3 deg. The van Leer limiter is also used for Cart3D to compute *dp/p*. Even if we cannot rigorously diagnose the *dp/p* differences in Fig. 4b, it is plausible to accept the grid resolution difference between the 1144 and 388 computed *dp/p* points at 3BL below the aircraft as a potential root cause.

The differences between the Cart3D and FUN3D solutions are irrelevant to the verification of approximate invariance of *dp/p* with respect to altitude change, but they are included to document the effects of viscosity on this supersonic configuration. The Cart3D and FUN3D solutions for AoA = 2.3 deg have C_L values (with a reference area of 3203 ft^2) of 0.0942 and 0.0960 at SOC, respectively, a relative difference of 1.9%. Note that, if the same C_L for inviscid and viscous analyses were required for *dp/p* calculation, the C_L difference of 1.9% would force Cart3D and FUN3D to use two different AoA values to compute *dp/p*, which could lead to more significant differences between the inviscid and viscous *dp/p* distributions due to the AoA difference for the inviscid and viscous solvers from the same C_L.

The FUN3D C_L is approximately invariant with altitude. The maximum relative difference between the FUN3D C_L values for the three altitudes listed in Fig. 4b is only 0.15%. The FUN3D drag coefficient values for these three altitudes differ slightly, ranging from 0.01460 for an altitude of 40,000 ft to 0.01526 for an altitude of 60,000 ft, with a maximum relative difference of 4.4%. The FUN3D lift-to-drag ratio (*L/D*) is 6.4, the low-fidelity *L/D* is 7.7 [4], and the Cart3D *L/D* is 10.1 for the Mach 1.7 46-PAX concept when cruise Mach = 1.7, cruise altitude = 51,740 ft, and AoA = 2.3 deg.

So, based on the approximate invariance of *dp/p* with respect to altitude change, the overland mission profile with a fixed low-boom cruise altitude (see Fig. 5 in Ref. [5]) is replaced by the low-boom mission profile in Fig. 5 for sonic boom and mission performance analyses. This low-boom mission profile is optimal for the low-boom requirement based on the following two facts: (i) the sonic boom from the aircraft is loudest at SOC and (ii) the required AoA change at the end of cruise has the smallest deviation from the SOC AoA when compared with any other mission profile, so that the aircraft has the best chance to retain the low-boom characteristics designed for the SOC AoA.

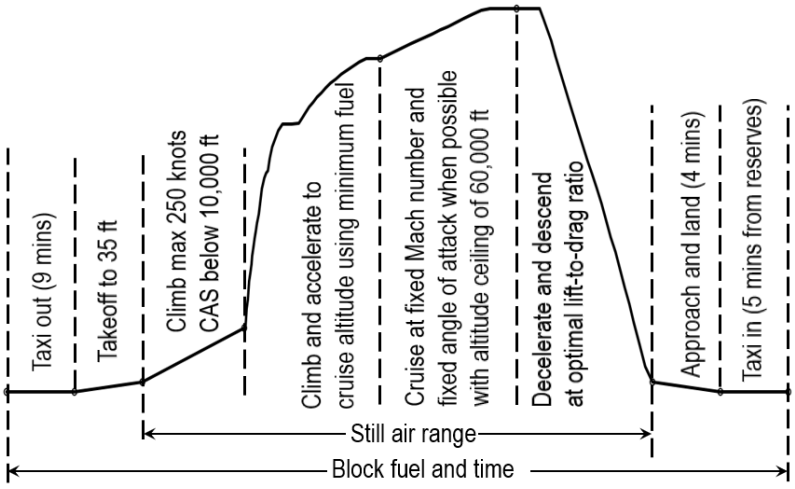

Fig. 5 Low-boom mission profile using a fixed AoA for cruise.

Note that the fixed AoA trajectory is approximately identical to a constant C_L trajectory. It is well known that the trajectory with a constant cruise speed and a properly selected constant C_L is commonly used for maximizing the cruise range based on the Breguet range equation (see Ref. [18]). For example, a constant C_L mission profile is specified in Fig. 9 of Ref. [19] to generate a high-performance supersonic concept with a range of 4000 nmi as a baseline for adjoint-based low-boom inverse design optimization. So, a fixed AoA trajectory itself is not a new idea. However, there is a fundamental difference between these two trajectory choices. The constant C_L for maximum range is typically determined by an approximately maximum *L/D* ratio of the aircraft (see the paragraph after Eq. (4) in Ref. [18]), whereas the derived C_L from the fixed AoA trajectory is not necessarily related to the maximum *L/D* ratio of the aircraft. The derived C_L is indirectly determined based on the AoA required to maintain the designed low-boom characteristics of the aircraft. Moreover, there is also a theoretical difference between a fixed AoA trajectory and a constant C_L trajectory. The fixed AoA trajectory defines a unique flow physics problem of an unchanged OML shape flying forward in a fixed orientation during the cruise. This is consistent with the physics for sonic boom modeling: capturing the flow physics of how air is displaced around a flying object that has a unique shape/orientation to create a specific air disturbance pattern on the ground. In contrast, a constant C_L trajectory means that the orientation of the OML shape flying forward depends on the flow solver due to a potential difference of the AoA values for inviscid and viscous solvers. If the same constant C_L were required for *dp/p* analysis, the Cart3D and FUN3D C_L difference of 1.9% for the Mach 1.7 46-PAX concept would lead to two different AoA values for the same C_L, which effectively corresponds to two different OML shapes flying forward for sonic boom analyses.

The optimality of the fixed AoA trajectory for cruise range of the Mach 1.7 46-PAX concept is mainly due to the simultaneous optimization of low-boom and mission performance goals using the BCO method [4] that generates the OML of this concept. As a result, the *L/D* of the Mach 1.7 46-PAX concept at SOC is indirectly maximized under the low-boom constraint. So, the low-boom mission profile also optimizes the overland cruise performance of this concept under the low-boom constraint using the derived C_L from the fixed AoA for cruise. Table 1 includes some weight and performance data for the Mach 1.7 46-PAX concept. If the mission profile for overland flight used a fixed cruise altitude of 51,740 ft, then the overland range would be 3314 nmi instead of the 3725 nmi achieved using the fixed

AoA cruise as shown in Table 1. In general, if a low-boom aircraft's *L/D* is maximized under the low-boom constraint at SOC, then the derived C_L trajectory approximately maximizes the overland range [18] because the *L/D* values for the cruise are close or identical (without viscosity) to the maximized *L/D* at SOC.

Table 1 Mach 1.7 46-PAX concept

Variable	Value	Variable	Value
Seat pitch, in	38	Low-boom angle of attack, deg	2.30
Max takeoff gross weight, lb	147,600	Altitude at start of low-boom cruise, ft	51,740
Zero fuel weight, lb	75,683	PLdB of low-boom inverse design target	69.9
Overwater cruise Mach	1.8	Weight at start of overland cruise, lb	136,643
Overland cruise Mach	1.7	Block fuel for maximum range, lb	64,655
Takeoff field length, ft	8504	Unrestricted overwater range, nmi	3671
Approach velocity, kts	126	Low-boom overland range, nmi	3725

There are several technical issues in this section that need further discussion. First, in Table 1, the low-boom overland range of 3725 nmi is longer than the unrestricted overwater range of 3671 nmi, which might give a false impression that the low-boom constraint does not incur any penalty to the aircraft cruise performance. There are two reasons for this abnormality in this case: (i) during the MDO of the OML of the Mach 1.7 46-PAX concept, the takeoff gross weight for the overland mission is minimized for optimal cruise efficiency for the overland cruise Mach of 1.7 without any consideration of the unrestricted overwater cruise efficiency (see Ref. [4]) and (ii) the unrestricted overwater cruise Mach of 1.8 is higher than the overland cruise Mach of 1.7. The reason for using the cruise Mach of 1.7 instead of 1.8 for low-boom supersonic overland flights was to increase the overland cruise efficiency with a slower cruise speed [4]. The combined effect is that, for the same aircraft weight at SOC and the same cruise distance, the overwater cruise fuel burn for Mach 1.8 at the optimal cruise altitudes is still slightly higher than the overland cruise fuel burn for Mach 1.7 with fixed AoA. However, for the same MTOGW, the unrestricted overwater range for a cruise Mach of 1.7 is longer than the low-boom overland range in Table 1. The low-boom penalty on cruise performance is manifested in both the aircraft design and operations: (i) the low-boom constraint significantly reduces the feasible design space for aircraft performance and (ii) the low-boom mission profile might be slightly different from the unconstrained optimal cruise flight due to the altitude constraint derived from the fixed AoA.

Second, it is worth noting that the sonic boom ground noise level is very sensitive to the small differences between the $A_{e,r}$ of the aircraft and the low-boom target, as shown in Fig. 2. In this design case, the designed aircraft PLdB is more than 20 PLdB higher than the target. However, this is an appropriate conceptual-level low-boom constraint corresponding to a higher fidelity low-boom constraint of an undertrack sonic boom ground noise level about 75 to 79 PLdB for the aircraft at SOC, very much in line with the expected ground PLdB level of the X-59 [1,2]. In fact, CFD-based low-boom inverse design methods were demonstrated to be capable of reducing the PLdB difference between the target and the aircraft to within 5 to 9 PLdB [20-23]. The introduction section in Ref. [4] outlines the theoretical feasibility of eliminating the inverse design error between the low-boom target and $A_{e,r}$ of the aircraft with lift and volume equivalent area modifications that have approximately the same magnitudes as the inverse design errors. The combination of the demonstrated CFD-based inverse design capabilities and the inverse design theory for $A_{e,r}$ indicates that a minor lift and volume modification of a low-boom concept generated by the BCO method for a target PLdB of 70 has the potential to reduce the resulting aircraft's undertrack sonic boom ground noise level to a range of 75 to 79 PLdB, achieving the low-boom and mission performance goals at a higher fidelity level. The uncertainty here is whether the desired mission performance goals would be adversely affected by "minor" OML modifications, which requires further research.

III. Assessment of Low-Boom Characteristics for Cruise Segment

In this paper, the undertrack low-boom characteristics of a supersonic aircraft are defined by the sonic boom ground noise level of an $A_{e,r}$ target that can be approximately matched by the aircraft's $A_{e,r}$ at a given cruise condition for the low-boom mission profile in Fig. 5. The $A_{e,r}$ of the aircraft [7] is obtained by reversely propagating the off-body pressure at 3BL to 50 ft below the aircraft using an augmented Burgers equation, converting the reversely propagated pressure to Whitham's *F*-function [24], and calculating the corresponding equivalent area of Whitham's *F*-function. The details for calculating the $A_{e,r}$ in the undertrack direction can be found in Ref. [25].

The assessment of undertrack low-boom characteristics of a supersonic aircraft at any cruise condition is formulated as the following multiobjective optimization problem for simultaneous minimization of the ground noise level of an $A_{e,r}$ target, denoted by A_e, and the difference between A_e and the aircraft's $A_{e,r}$, denoted by $\|A_e - A_{e,r}\|$.

$$\min_{\boldsymbol{d}} \left\{ \mathrm{PLdB}(A_e), \|A_e - A_{e,r}\| \right\} \tag{1}$$

The notation PLdB(A_e) represents the PLdB value of the undertrack ground signature of A_e. The notation $\|f\|$ is the 2-norm of a function f on interval [0, l_e], which equals $\left(\int_0^{l_e} |f(t)|^2 \, dt \,/ l_e\right)^{\frac{1}{2}}$. The symbol l_e is the effective length of a supersonic configuration, which is the largest effective distance (x_e) where the Mach angle cut plane intersects the configuration. The A_e in Eq. (1) is parameterized by the control points of a Bezier curve. For a parameter t between 0 and 1, the corresponding point (x, $A_e(x)$) on a Bezier curve is defined as follows.

$$\begin{aligned} x(t) &= l_e \cdot t^9 + \sum_{j=1}^{8} x_{c,j} \cdot \frac{9!}{j!\,(9-j)!} \cdot t^j \cdot (1-t)^{9-j} \\ A_e\big(x(t)\big) &= y_{c,8} \cdot t^9 + \sum_{j=2}^{8} y_{c,j} \cdot \frac{9!}{j!\,(9-j)!} \cdot t^j \cdot (1-t)^{9-j} \end{aligned} \tag{2}$$

Here, a Bezier curve with 10 control points is used as a parametric form of A_e. In Refs. [4,5,25], the parametric form of an $A_{e,r}$ target has only 8 control points. However, the George-Seebass-Darden low-boom inverse design theory [26,27] implicitly depends on the validity of the inverse relation between an equivalent area and an F-function (see Theorems 1 and 2 in Ref. [28]). This inverse relation is valid if and only if the slope of the equivalent area is zero at $x_e = 0$ and $x_e = l_e$ (see Remark 2 after Theorem 1 in Ref. [28]). So, theoretically, the slope of an $A_{e,r}$ target must be zero at $x_e = 0$ and $x_e = l_e$, even though minor deviations of the slope from zero at $x_e = 0$ and $x_e = l_e$ could be considered as acceptable numerical errors for low-boom inverse design of $A_{e,r}$. To be consistent with the theory in Ref. [28], two additional control points are added to enforce the zero-slope constraints at $x_e = 0$ and $x_e = l_e$. The parametric form of A_e in Eq. (2) always satisfies the zero-slope constraint at $x_e = 0$ and $x_e = l_e$. The control points are defined by their coordinates $x_{c,j}$ and $y_{c,j}$. To keep the number of design variables for an $A_{e,r}$ target the same as before, $x_{c,1}$ and $x_{c,8}$ are fixed with $x_{c,1} = 0.001 \cdot l_e$ and $x_{c,8} = 0.999 \cdot l_e$ in this paper. The design vector $\boldsymbol{d}$ in Eq. (1) has $x_{c,j}$ ($2 \le j \le 7$) and $y_{c,j}$ ($2 \le j \le 8$) as the components with a total of 13 design variables. The choices for the resulting parametric form of an $A_{e,r}$ target are empirical. But this parametric form is adequate for the applications in this paper. That is, every $A_{e,r}$ in this paper can be fitted by an A_e with $\|A_e - A_{e,r}\| \le \epsilon$, where ϵ is an acceptable error tolerance. If this parametric form were not flexible enough for $A_{e,r}$ targets, $x_{c,1}$ and $x_{c,8}$ could also be used as design variables in Eq. (1). If needed, more control points could be used to define an $A_{e,r}$ target in Eq. (1). But the time required to solve Eq. (1) increases with more design variables.

The selected optimal solution of Eq. (1) as the inverse design target for $A_{e,r}$ is the Pareto optimal solution with the minimum value of PLdB(A_e) while the inverse design error of $A_{e,r}$ for the selected $A_{e,r}$ target is within the error tolerance, i.e., $\|A_e - A_{e,r}\| \le \epsilon$. For easy reference, this Pareto optimal solution will be denoted by $A_{e,r}^{\mathrm{target}}$. In this paper, the acceptable error tolerance ϵ is $0.007 \cdot A_{e,r}(l_e)$, which was used in Refs. [4,5]. Theoretically, $A_{e,r}^{\mathrm{target}}$ is equivalent to the optimal solution that minimizes PLdB(A_e) subject to the constraint $\|A_e - A_{e,r}\| \le \epsilon$. In practice, it is more difficult to solve this constrained single-objective optimization problem using a genetic algorithm than solving Eq. (1). This is because small changes of the design variables can change the A_e curve shape significantly and lead to a violation of the constraint $\|A_e - A_{e,r}\| \le \epsilon$. Moreover, the Pareto front provides a trade-off option between the required inverse design error tolerance and the target PLdB when an exact value of ϵ is not critical. Note that Eq. (1) is not formulated to solve a low-boom inverse design optimization problem. Instead, it is formulated to quantify the lowest ground noise level of A_e that could be used as a low-boom target for which the aircraft's $A_{e,r}$ is an acceptable inverse design.

Equation (1) is solved using the non-dominated sorting genetic algorithm II (NSGA II) in ModelCenter [29]. NSGA II requires finite lower and upper bounds for the design variables. The target $A_{e,r}^{\mathrm{target}}$ could be obtained by solving Eq. (1) with a set of bound constraints on $\boldsymbol{d}$: $0 \le x_{c,j} \le l_e$ and $0 \le y_{c,j} \le 1.5 \cdot A_{e,r}(l_e)$. In practice, more restrictive bounds of $\boldsymbol{d}$ are used empirically to reduce the size of the design space in search of $A_{e,r}^{\mathrm{target}}$.

If $A_{e,r}$ is an acceptable inverse design for $A_{e,r}^{\mathrm{target}}$, then the underlying configuration has the potential to achieve a ground noise level of PLdB($A_{e,r}^{\mathrm{target}}$) at the specified cruise condition. Otherwise, the underlying configuration without

any shape modification is not considered to have any quantifiable low-boom characteristics at the specified cruise condition. In this case, a more flexible parametric model of A_e is required for assessment of low-boom characteristics of the underlying supersonic configuration for the required inverse design error constraint. It is worth pointing out that this analysis method can also be applied to analyze low-boom characteristics of a low-boom concept in an off-track direction at any cruise condition (see the full version of this paper [30]).

Recall that *dp/p* at 3BL below the aircraft with a fixed AoA is approximately identical at any cruise altitude. As a result, the Mach 1.7 46-PAX concept is an acceptable low-boom inverse design for the same undertrack $A_{e,r}$ target in Fig. 2 at any cruise condition before it changes the AoA after reaching the cruise ceiling in the low-boom mission profile. For the same *dp/p*, the corresponding ground signature has a lower noise level if the cruise altitude is higher, which is based on our numerical verifications of a variety of *dp/p* shapes. An intuitive interpretation is that the loudness of sonic boom generated by a fixed *dp/p* decreases as the propagation distance increases. So, the ground noise level of the same $A_{e,r}$ target decreases when the cruise altitude increases (compare the signatures in Figs. 2 and 3). Further research is required to fully confirm the correctness of this empirical conclusion.

After reaching the cruise ceiling of 60,000 ft, the Mach 1.7 46-PAX concept must reduce the AoA to match the reduced cruise weight as the fuel is consumed during the cruise. At the end of cruise, the AoA is reduced to 2.1 deg. The undertrack $A_{e,r}$ of the Mach 1.7 46-PAX concept at the end of cruise is very different from the $A_{e,r}$ target at SOC, as expected. However, the proposed analysis method shows that the Mach 1.7 46-PAX concept is an acceptable inverse design for an undertrack $A_{e,r}$ target at 60,000 ft with sonic boom ground noise level of 66.0 PLdB (see Fig. 6). This shows that the Mach 1.7 46-PAX concept has low-boom $A_{e,r}$ shapes in the undertrack direction as acceptable inverse designs with target ground noise levels below 70 PLdB for the entire cruise segment (see Figs. 2, 3, and 6).

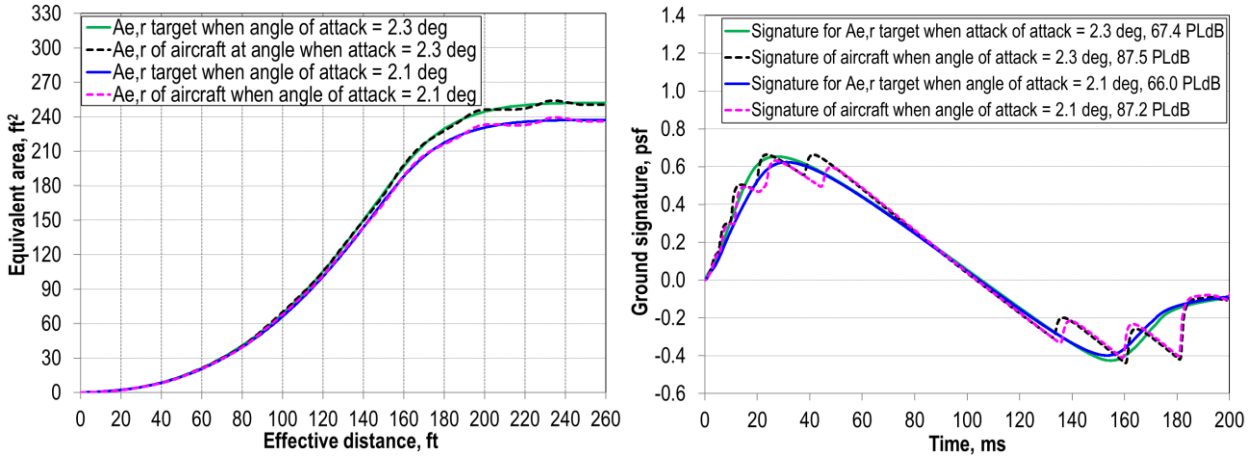

Fig. 6 $A_{e,r}$ distributions and signatures of the aircraft cruising at 60,000 ft in undertrack direction.

The effects of AoA, Mach, and altitude are considered in our sonic boom analysis of the same aircraft OML for the entire cruise segment. For a realistic cruise flight, the center of gravity (CG) is another important parameter for trim control that could change the aircraft OML and the low-boom characteristics. If the CG is not aligned properly with the center of aerodynamic pressure (CP) for the designed low-boom OML, then control surface deflections are required to achieve a trim condition, i.e., CG = CP. Any control surface deflection will change the OML of the aircraft and its *dp/p* at 3BL below the aircraft. Fortunately, one can implicitly incorporate the trim constraint into the low-boom $A_{e,r}$ target as discussed in Ref. [25]. The resulting inverse design solution will automatically satisfy the trim condition at SOC via a fuel distribution (see Ref. [4]). The trim constraint for the sonic boom analysis is beyond the scope of this paper. Coupling the sonic boom analysis with a fuel redistribution for trim is more appropriate during the preliminary design phase when the aircraft structural layout and the detailed fuel tank arrangement are available.

IV. Conclusions

An optimal mission profile, called the low-boom mission profile, is proposed for low-boom supersonic aircraft. The low-boom mission profile uses a fixed AoA for the cruise segment until reaching the cruise ceiling. The fixed AoA is determined by the cruise condition for the low-boom shaping of the aircraft. The derived C_L trajectory is not necessarily the optimal trajectory for the cruise range when unrestricted supersonic flight is allowed. The undertrack sonic boom ground noise level is reduced during the cruise because of the increasing altitude from the fixed AoA trajectory and the approximate invariance of nondimensional overpressure at 3BL below a supersonic aircraft with

respect to cruise altitude change when the AoA and cruise Mach are fixed. The approximate invariance of nondimensional overpressure at 3BL below a supersonic aircraft is verified using both Euler and Reynolds-averaged Navier-Stokes CFD solvers. A low-boom supersonic transport concept is used to illustrate that, compared to the fixed cruise altitude trajectory, the low-boom mission profile can increase the cruise range of a low-boom aircraft and reduce the undertrack sonic boom ground noise levels for the entire cruise segment.

One significant contribution of this paper is the implication that an aircraft OML satisfying a sonic boom ground noise level constraint at SOC will satisfy the same noise level constraint over the entire cruise segment, as long as a fixed AoA trajectory is flown.

Acknowledgments

This work is funded by the NASA Commercial Supersonic Technology Project.

References

[1] Rathsam, J, Coen, P., Loubeau, A, Ozoroski, L., and Shah, G., "Scope and Goals of NASA's Quesst Community Test Campaign with the X-59 Aircraft," *14th ICBEN Congress on Noise as a Public Health Problem*, Belgrade, Serbia, June 2023, (organized by International Commission on Biological Effects of Noise, Gothenburg, Sweden). URL:icben2023.com/download-paper/presenting63.pdf [retrieved 14 Feb. 2024]

[2] Doebler, W., Wilson, S., Loubeau, A., and Sparrow, V., "Simulation and Regression Modeling of NASA's X-59 Low-Boom Carpets Across America," *Journal of Aircraft*, Vol. 60, No. 2, 2023, pp. 280–593. doi:10.2514/1.C036876 (See Fig. 6)

[3] Stevens, S., "Perceived Level of Noise by Mark VII and Decibels (E)," *Journal of the Acoustical Society of America*, Vol. 51, No. 2B, 1972, pp. 575–601. doi:10.1121/1.1912880

[4] Li, W., and Geiselhart, K., "Multi-objective, Multidisciplinary Optimization of Low-Boom Supersonic Transports Using Multifidelity Models," *Journal of Aircraft*, Vol. 59, No. 5, 2022, pp. 1137–1151. doi:10.2514/1.C036656.

[5] Li, W., and Geiselhart, K., "Propulsion-Airframe Integration for Conceptual Redesign of a Low-Boom Supersonic Transport," *Journal of Aircraft*, Vol. 61, No. 2, 2024, pp. 331–344. doi:10.2514/1.C037310

[6] Morgenstern, J., Norstrud, N., Stelmack, M., and Jha, P., "Advanced Concept Studies for Supersonic Commercial Transports Entering Service in 2030-2035 (N+3)," AIAA Paper 2010-5114, June 2010. doi:10.2514/6.2010-5114

[7] Li, W., and Rallabhandi, S., "Inverse Design of Low-Boom Supersonic Concepts Using Reversed Equivalent-Area Targets," *Journal of Aircraft*, Vol. 51, No. 1, 2014, pp. 29–36. doi:10.2514/1.C031551

[8] Ishikawa, H., Ueno, A., Koganezawa, S., Makino, Y., Liebhardt, B., and Lütjens, K., "Sensitivity Study and Primary Boom Carpet Assessment for Conceptual Low Boom Supersonic Transport," AIAA Paper 2021-0608, Jan. 2021. doi:10.2514/6.2021-0608

[9] McCullers, L., *FLOPS User's Guide*, NASA Langley Research Center, Hampton, Virginia, 2011 (available with public distribution of software).

[10] *Cart3D, Version 1.5*, NASA, URL:https://www.nas.nasa.gov/software/cart3d.html [retrieved Feb. 2024].

[11] *FUN3D, Version 14.0.2*, NASA, URL:http://fun3d.larc.nasa.gov, [retrieved Feb. 2024].

[12] *HeldenMesh*, Helden Aerospace, URL:https://heldenaero.com/heldenmesh [retrieved Feb. 2024].

[13] Park, M., Campbell, R., Elmiligui, A., Cliff, S., and Nayani, S., "Specialized CFD Grid Generation Methods for Near-Field Sonic Boom Prediction," AIAA Paper 2014-0115, Jan. 2014. doi:10.2514/6.2014-0115

[14] Spalart, P., and Allmaras, S., "A One-Equation Turbulence Model for Aerodynamic Flows," *La Recherche Aérospatiale*, Vol. 1, No. 1,1994, pp. 5–21.

[15] Roe, P., "Approximate Riemann Solvers, Parameter Vectors, and Difference Schemes," *Journal of Computational Physics*, Vol. 43, No. 2,1981, pp. 357–372. doi:10.1016/0021-9991(81)90128-5

[16] Van Leer, B., "Towards the Ultimate Conservative Difference Scheme. II. Monotonicity and Conservation Combined in a Second-Order Scheme," *Journal of Computational Physics*, Vol. 14, No. 4, 1974, pp. 361–370. doi:10.1016/0021-9991(74)90019-9

[17] Ordaz, I., and Li, W., "Integration of Off-Track Sonic Boom Analysis in Conceptual Design of Supersonic Aircraft," *Journal of Aircraft*, Vol. 51, No. 1, 2014, pp. 23–28. doi:10.2514/1.C031511

[18] Teren, F., and Daniele, C., "Optimal Cruise Trajectories for Supersonic Airplanes," NASA TN D-6707, Mar. 1972.

[19] Wintzer, M., Kroo, I., Aftosmis, M., and Nemec, M., "Conceptual Design of Low Sonic Boom Aircraft Using Adjoint-Based CFD," *Proceedings of the Seventh International Conference on Computational Fluid Dynamics*, ICCFD7-2005, Big Island, HI, USA, July 2012. URL:https://www.nas.nasa.gov/publications/software/docs/cart3d/pages/publications/ICCFD7-2005_final.pdf [retrieved Feb. 2024].

[20] Aftosmis, M., Nemec, M., and Cliff, S., "Adjoint-Based Low-Boom Design with Cart3D," AIAA Paper 2011-3500, June 2011. doi:10.2514/6.2011-3500

[21] Rallabhandi, S., "Application of Adjoint Methodology to Supersonic Aircraft Design Using Reversed Equivalent Areas," *Journal of Aircraft*, Vol. 51, No. 6, 2014, pp. 1873–1882. doi:10.2514/1.C032518

[22] Wintzer, M., Ordaz, I., and Fenbert, J., "Under-Track CFD-Based Shape Optimization for a Low-Boom Demonstrator Concept," AIAA Paper 2015-2260, June 2015. doi:10.2514/6.2015-2260

[23] Li, W., "Feasibility of Supersonic Aircraft Concepts for Low-Boom and Flight Trim Constraints," AIAA Paper 2015-2581, June 2015. doi:10.2514/6.2015-2581

[24] Whitham, G., "On the Propagation of Weak Shock Waves," *Journal of Fluid Mechanics*, Vol. 1, No. 3, 1956, pp. 290–318. doi:10.1017/S0022112056000172

[25] Li, W., "Equivalent Area Targets for Inverse Design Optimization with Changing Low-Boom Cruise Conditions," *AIAA Journal*, Vol. 61, No. 3, 2023, pp. 1260–1269. doi:10.2514/1.J062324

[26] Seebass, R., and George, A., "Sonic Boom Minimization," *Journal of the Acoustical Society of America*, Vol. 51, No. 2C, 1972, pp. 686–694. doi:10.1121/1.1912902

[27] Darden, C., "Minimization of Sonic-Boom Parameters in Real and Isothermal Atmospheres," NASA TN D-7842, March 1975.

[28] Li, W., "A Theoretical and Computational Revisit of Conversions Between Whitham's F-Function and Equivalent Area," NASA/TM-20230002114, May 2023.

[29] *ModelCenter, Version 12.0*, Phoenix Integration Inc., URL:http://www.phoenix-int.com [retrieved Feb. 2024].

[30] Li, W., and Geiselhart, K., "Assessment of Off-Design Low-Boom Characteristics of a Low-Boom Supersonic Transport," AIAA Paper 2024-1875, Jan. 2024. doi:10.2514/6.2024-1875